

# Maximum Constant Boost Control of the Z-Source Inverter

Miaosen Shen<sup>1</sup>, Jin Wang<sup>1</sup>, Alan Joseph<sup>1</sup>, Fang Z. Peng<sup>1</sup>, Leon M. Tolbert<sup>2</sup>, and Donald J. Adams<sup>3</sup>

<sup>1</sup>Michigan State University

Department of Electrical and Computer Engineering

2120 Engineering Building, East Lansing, MI 48824

Phone: 517-432-3331, Fax: 517-353-1980, Email: [fzpeng@egr.msu.edu](mailto:fzpeng@egr.msu.edu)

<sup>2</sup>University of Tennessee, <sup>3</sup>Oak Ridge National Laboratory

**Abstract:** This paper proposes two maximum constant boost control methods for the Z-source inverter, which can obtain maximum voltage gain at any given modulation index without producing any low-frequency ripple that is related to the output frequency. Thus the Z-network requirement will be independent of the output frequency and determined only by the switching frequency. The relationship of voltage gain to modulation index is analyzed in detail and verified by simulation and experiment.

**Keywords-** Z-source inverter; PWM; Voltage boost;

## I. INTRODUCTION

In a traditional voltage source inverter, the two switches of the same phase leg can never be gated on at the same time because doing so would cause a short circuit (shoot-through) to occur that would destroy the inverter. In addition, the maximum output voltage obtainable can never exceed the dc bus voltage. These limitations can be overcome by the new Z-source inverter [1], shown in Fig. 1, that uses an impedance network (Z-network) to replace the traditional dc link. The Z-source inverter advantageously utilizes the shoot-through states to boost the dc bus voltage by gating on both the upper and lower switches of a phase leg. Therefore, the Z-source inverter can buck and boost voltage to a desired output voltage that is greater than the available dc bus voltage. In addition, the reliability of the inverter is greatly improved because the shoot-through can no longer destroy the circuit. Thus it provides a low-cost, reliable, and highly efficient single-stage structure for buck and boost power conversion.

The main circuit of the Z-source inverter and its operating principle have been described in [1]. Maximum boost control is presented in [2]. In this paper, we will present two control methods to achieve maximum voltage boost/gain while maintaining a constant boost viewed from the Z-source network and producing no low-frequency ripple associated with the output frequency. This maximum constant boost control can greatly reduce the  $L$  and  $C$  requirements of the Z-network. The relationship of voltage boost and modulation index, as well as the voltage stress on the devices, will be investigated.

## II. VOLTAGE BOOST, STRESS AND CURRENT RIPPLE

As described in [1], the voltage gain of the Z-source inverter can be expressed as

$$\frac{\hat{V}_o}{V_{dc}/2} = MB, \quad (1)$$

where  $\hat{V}_o$  is the output peak phase voltage,  $V_{dc}$  is the input dc voltage,  $M$  is the modulation index, and  $B$  is the boost factor.  $B$  is determined by

$$B = \frac{1}{1 - 2\frac{T_0}{T}}, \quad (2)$$

where  $T_0$  is the shoot-through time interval over a switching cycle  $T$ , or  $\frac{T_0}{T} = D_0$  is the shoot-through duty ratio.

In [1], a simple boost control method was used to control the shoot-through duty ratio. The Z-source inverter maintains the six active states unchanged as in traditional carrier-based pulse width modulation (PWM) control. In this case, the shoot-through time per switching cycle is constant, which means the boost factor is a constant. Therefore, under this condition, the dc inductor current and capacitor voltage have no ripples that are associated with the output frequency. As has been examined in [2], for this simple boost control, the obtainable shoot-through duty ratio decreases with the increase of  $M$ , and the resulting voltage stress across the devices is fairly high. To obtain the maximum voltage boost, [2] presents the maximum boost control method as shown in Fig. 2, which shoots through all zero-voltage vectors entirely. Based on the map in Fig. 2, the shoot-through duty cycle  $D_0$  varies at six times the output frequency. As can be seen from [2], the voltage boost is inversely related to the shoot-through duty ratio; therefore, the ripple in shoot-through duty ratio will result in ripple in the current through the inductor, as well as in the voltage across the capacitor. When the output frequency is low, the inductor current ripple becomes significant, and a large inductor is required.

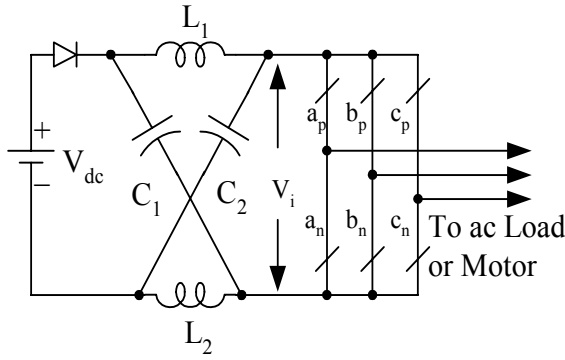


Fig. 1 Z-source inverter

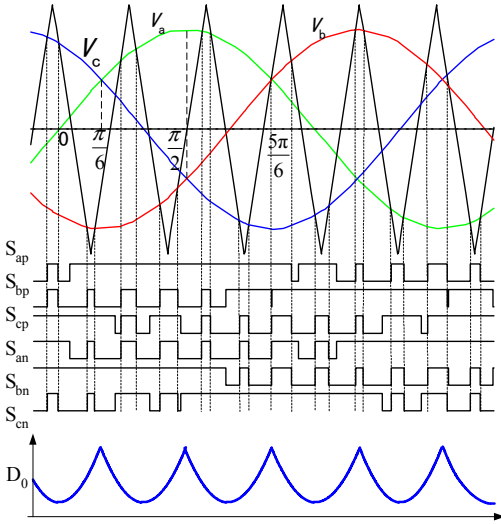


Fig. 2 Maximum boost control sketch map

To calculate the current ripple through the inductor, the circuit can be modeled as in Fig. 3, where  $L$  is the inductor in the Z-source network,  $V_c$  is the voltage across the capacitor in the Z-source network, and  $V_i$  is the voltage fed to the inverter. Neglecting the switching frequency element, the average value of  $V_i$  can be described as

$$\bar{V}_i = (1 - D_0) * BV_{dc} \quad (3)$$

From [2], we have

$$D_0(\theta) = \frac{2 - (M \sin \theta - M \sin(\theta - \frac{2}{3}\pi))}{2} \quad (4)$$

$$= 1 - \frac{\sqrt{3}}{2} M \cos(\theta - \frac{1}{3}\pi) \quad (\frac{\pi}{6} < \theta < \frac{\pi}{2})$$

and  $B = \frac{\pi}{3\sqrt{3}M - \pi} \quad (5)$

As can be seen from Eq. (4),  $D_0$  has maximum value when  $\theta = \frac{\pi}{3}$  and has minimum value when  $\theta = \frac{\pi}{6}$  or  $\theta = \frac{\pi}{2}$ . If

we suppose the voltage across the capacitor is constant, the voltage ripple across the inductor can be approximated as a sinusoid with peak-to-peak value of

$$V_{pk2pk} = V_{i \max} - V_{i \min}$$

$$= (\frac{\sqrt{3}}{2}M - \frac{\sqrt{3}}{2}M \cos(\frac{\pi}{6})) * BV_{dc} \quad (6)$$

$$= \frac{(\frac{\sqrt{3}}{2} - \frac{3}{4})M\pi}{3\sqrt{3}M - \pi} V_{dc}$$

If the output frequency is  $f$ , the current ripple through the inductor will be

$$\Delta I_L = \frac{V_{pk2pk}}{2 * \pi * 6f * L} \quad (7)$$

$$= \frac{(\frac{\sqrt{3}}{2} - \frac{3}{4})MV_{dc}}{12 * (3\sqrt{3}M - \pi)fL}$$

As can be seen from Eq. (7), when the output frequency decreases, in order to maintain the current ripple in a certain range, the inductor has to be large.

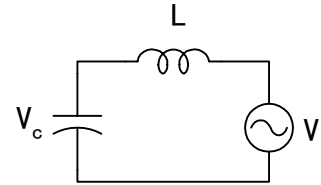


Fig. 3 Model of the circuit

### III. MAXIMUM CONSTANT BOOST CONTROL

In order to reduce the volume and cost, it is important always to keep the shoot-through duty ratio constant. At the same time, a greater voltage boost for any given modulation index is desired to reduce the voltage stress across the switches. Figure 4 shows the sketch map of the maximum constant boost control method, which achieves the maximum voltage gain while always keeping the shoot-through duty ratio constant. There are five modulation curves in this control method: three reference signals,  $V_a$ ,  $V_b$ , and  $V_c$ , and two shoot-through envelope signals,  $V_p$  and  $V_n$ . When the carrier triangle wave is greater than the upper shoot-through envelope,  $V_p$ , or lower than the lower shoot-through envelope,  $V_n$ , the inverter is turned to a shoot-through zero state. In between, the inverter switches in the same way as in traditional carrier-based PWM control.

Because the boost factor is determined by the shoot-through duty cycle, as expressed in [2], the shoot-through duty cycle must be kept the same in order to maintain a constant boost. The basic point is to get the maximum  $B$  while keeping it constant all the time. The upper and lower envelope curves are periodical and are three times

the output frequency. There are two half-periods for both curves in a cycle.

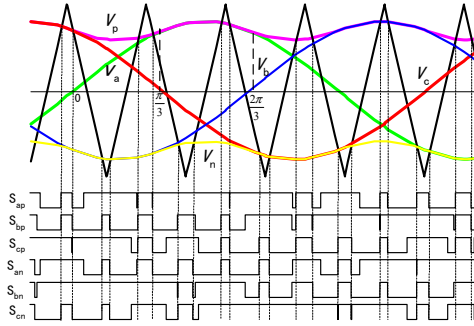


Fig. 4 Sketch map of constant boost control

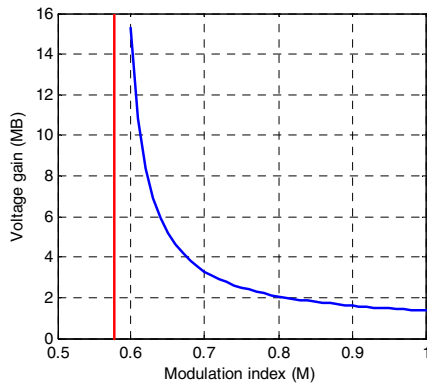


Fig. 5  $V_{ao}/0.5V_0$  versus  $M$

For the first half-period,  $(0, \pi/3)$  in Fig. 4, the upper and lower envelope curves can be expressed by Eqs. (8) and (9), respectively.

$$V_{p1} = \sqrt{3}M + \sin(\theta - \frac{2\pi}{3})M \quad 0 < \theta < \frac{\pi}{3} \quad (8)$$

$$V_{n1} = \sin(\theta - \frac{2\pi}{3})M \quad 0 < \theta < \frac{\pi}{3} \quad (9)$$

For the second half-period  $(\pi/3, 2\pi/3)$ , the curves meet Eqs. (10) and (11), respectively.

$$V_{p2} = \sin(\theta)M \quad \frac{\pi}{3} < \theta < \frac{2\pi}{3} \quad (10)$$

$$V_{n2} = \sin(\theta)M - \sqrt{3}M \quad \frac{\pi}{3} < \theta < \frac{2\pi}{3} \quad (11)$$

Obviously, the distance between these two curves is always constant, that is,  $\sqrt{3}M$ . Therefore the shoot-through duty ratio is constant and can be expressed as

$$\frac{T_0}{T} = \frac{2 - \sqrt{3}M}{2} = 1 - \frac{\sqrt{3}M}{2} \quad (12)$$

The boost factor  $B$  and the voltage gain can be calculated:

$$B = \frac{1}{1 - 2\frac{T_0}{T}} = \frac{1}{\sqrt{3}M - 1} \quad (13)$$

$$\frac{\hat{v}_o}{V_{dc}/2} = MB = \frac{M}{\sqrt{3}M - 1} \quad (14)$$

The curve of voltage gain versus modulation index is shown in Fig. 5. As can be seen in Fig. 5, the voltage gain approaches infinity when  $M$  decreases to  $\frac{\sqrt{3}}{3}$ .

This maximum constant boost control can be implemented using third harmonic injection [3]. A sketch map of the third harmonic injection control method, with 1/6 of the third harmonic, is shown in Fig. 6. As can be seen from Fig. 6,  $V_a$  reaches its peak value  $\frac{\sqrt{3}}{2}M$  while  $V_b$  is at its minimum value  $-\frac{\sqrt{3}}{2}M$ . Therefore, a unique feature can be obtained: only two straight lines,  $V_p$  and  $V_n$ , are needed to control the shoot-through time with 1/6 (16%) of the third harmonic injected.

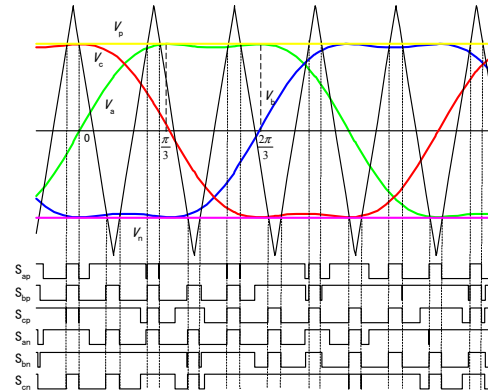


Fig. 6 Sketch map of constant boost control with third harmonic injection

The shoot-through duty ratio can be calculated by

$$\frac{T_0}{T} = \frac{2 - \sqrt{3}M}{2} = 1 - \frac{\sqrt{3}M}{2} \quad (15)$$

As we can see, it is identical to the previous maximum constant boost control method. Therefore, the voltage gain can also be calculated by the same equation. The difference is that in this control method, the range of  $M$  is increased to  $\frac{2}{3}\sqrt{3}$ . The voltage gain versus  $M$  is shown in Fig.7. The voltage gain can be varied from infinity to zero smoothly by increasing  $M$

from  $\frac{\sqrt{3}}{3}$  to  $\frac{2}{\sqrt{3}}$  with shoot-through states (solid curve in Fig. 7) and then decreasing  $M$  to zero without shoot-through states (dotted curve in Fig. 7).

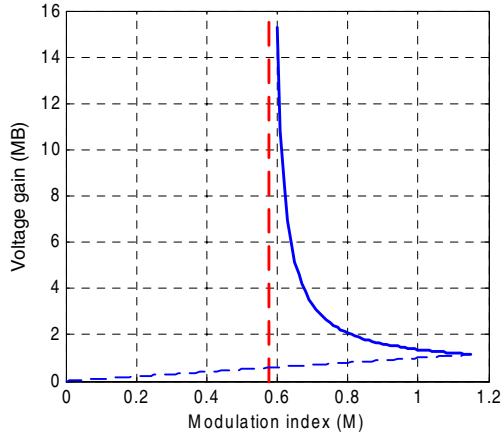


Fig. 7  $V_{ac}/0.5V_0$  versus  $M$

#### IV. VOLTAGE STRESS COMPARISON

As defined in [2], voltage gain  $G$  is

$$G = MB = \frac{M}{\sqrt{3M-1}} \quad (16)$$

We have

$$M = \frac{G}{\sqrt{3G-1}} \quad (17)$$

The voltage across the devices,  $V_s$ , can be expressed as

$$V_s = BV_{dc} = (\sqrt{3G-1})V_{dc} \quad (18)$$

The voltage stresses across the devices with different control methods are shown in Fig. 8.

As can be seen from Fig. 8, the proposed method will cause a slightly higher voltage stress across the devices than the maximum control method, but a much lower voltage stress than the simple control method. However, since the proposed method eliminates line frequency related ripple, the passive components in the Z-network will be smaller, which will be advantageous in many applications.

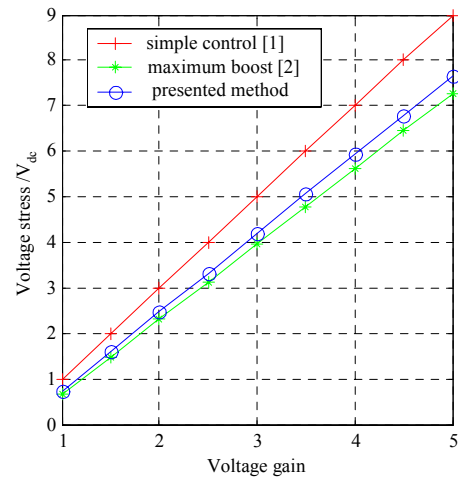


Fig. 8 Voltage stress comparison of different control methods

#### V. SIMULATION AND EXPERIMENTAL RESULTS

To verify the validity of the control strategies, simulation and experiments were conducted with the following parameters: Z-source network:  $L_1 = L_2 = 1$  mH (60 Hz inductor),  $C_1 = C_2 = 1,300$   $\mu$ F; switching frequency: 10 kHz; output power: 6 kW. The simulation results with the modulation index  $M = 0.812$ ,  $M = 1$ , and  $M = 1.1$  with third harmonic injection are shown in Figs. 9 through 11, respectively, where the input voltages are 145, 250, and 250 V, respectively. Table I lists the theoretical voltage stress and output line-to-line rms voltage based on the previous analysis.

Table I. Theoretical voltage stress and output voltage under different conditions

Operating condition	Voltage stress (V)	Output voltage $V_{L-L}$ (V)
$M = 0.812$ , $V_{dc} = 145$ V	357	177
$M = 1$ , $V_{dc} = 250$ V	342	209
$M = 1.1$ , $V_{dc} = 250$ V	276	186

The simulation results in Figs. 9–11 are consistent with the theoretical analysis, which verifies the previous analysis and the control concept.

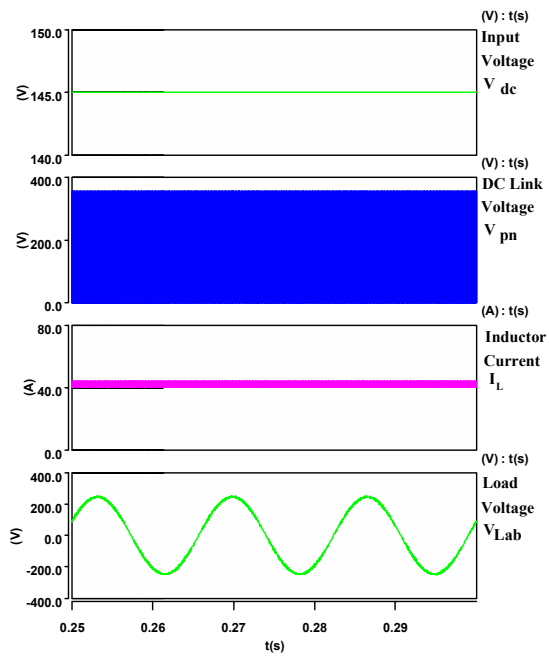


Fig. 9 Simulation results with  $M = 0.8$

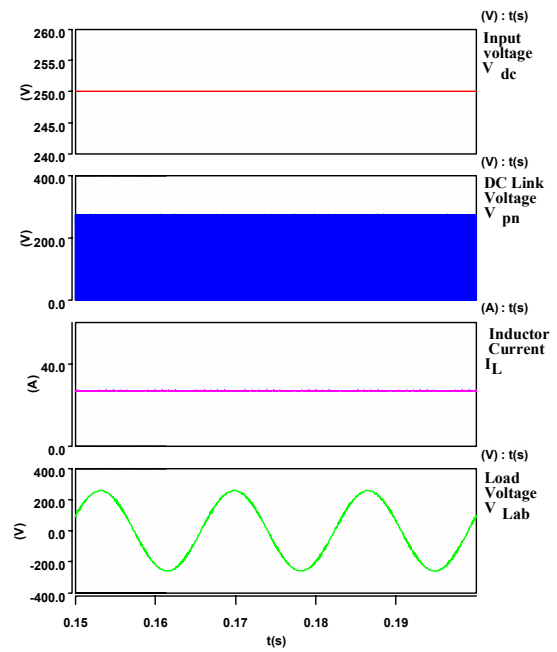


Fig. 11 Simulation results with  $M = 1.1$

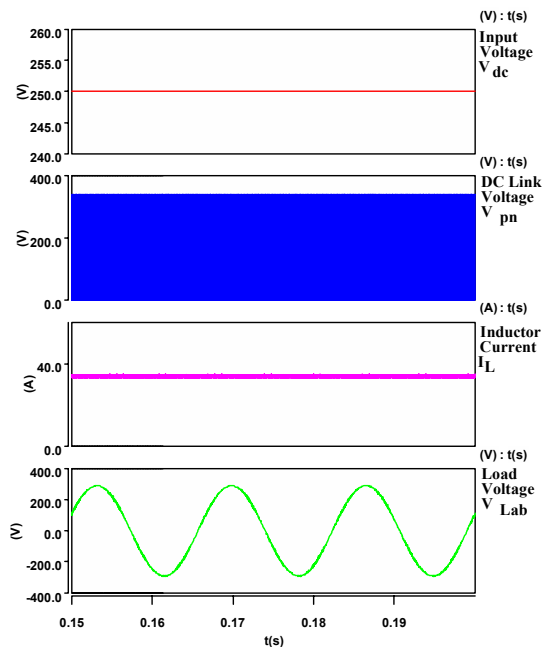


Fig. 10 Simulation results with  $M = 1$

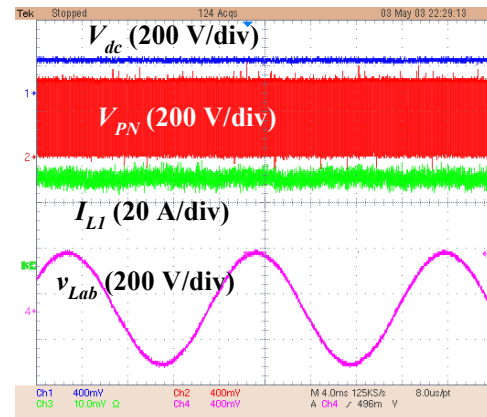


Fig. 12 Experimental results with  $V_{dc} = 145V$  and  $M = 0.812$

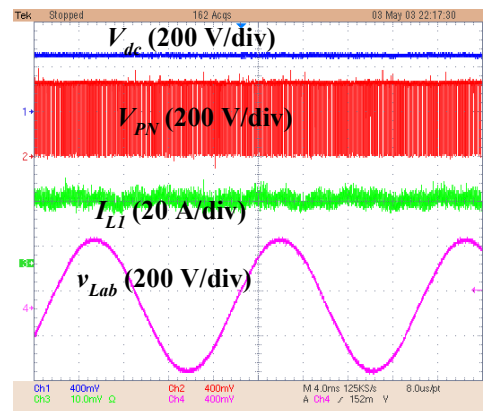


Fig. 13 Experimental results with  $V_{dc} = 250V$  and  $M = 1$

The experimental results with the same operating conditions are shown in Figs. 12, 13, and 14, respectively.

Based on these results, the experimental results agree with the analysis and simulation results very well. The validity of the control method is verified.

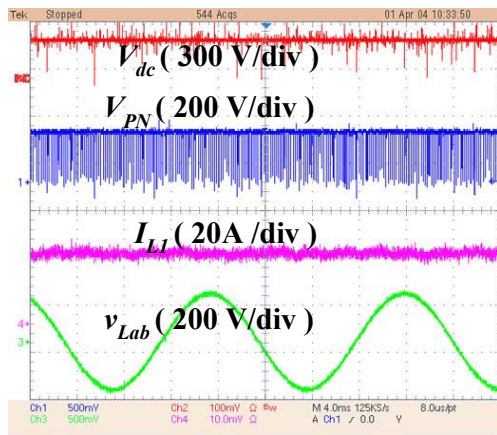


Fig. 14 Experimental results with  $V_{dc} = 250V$  and  $M = 1.1$

## VI. CONCLUSION

Two control methods to obtain maximum voltage gain with constant boost have been presented that achieve maximum voltage boost without introducing any low-frequency ripple related to the output frequency. The

relationship of the voltage gain and the modulation index was analyzed in detail. The different control methods have been compared. The proposed method can achieve the minimum passive components requirement and maintain low voltage stress at the same time. The control method has been verified by simulation and experiments.

## REFERENCES

- [1] F. Z. Peng, "Z-Source Inverter," *IEEE Transactions on Industry Applications*, **39**(2), pp. 504–510, March/April 2003.
- [2] F. Z. Peng and Miaosen Shen, Zhaoming Qian, "Maximum Boost Control of the Z-source Inverter," in *Proc. of IEEE PESC 2004*.
- [3] D.A. Grant and J. A. Houldsworth: PWM AC Motor Drive Employing Ultrasonic Carrier. *IEE Conf. PE-VSD*, London, 1984, pp. 234-240.
- [4] Bimal K. Bose, *Power Electronics and Variable Frequency Drives*, Upper Saddle River, NJ: Prentice-Hall PTR, 2002.
- [5] P. T. Krein, *Elements of Power Electronics*, London, UK: Oxford Univ. Press, 1998.
- [6] W. Leonard, *Control of Electric Drives*, New York: Springer-Verlag, 1985